Sensors & Actuators: B. Chemical 287 (2019) 191–198

Contents lists available at ScienceDirect

Sensors and Actuators B: Chemical

journal homepage: www.elsevier.com/locate/snb

Fabrication of highly sensitive and selective room-temperature nitrogen dioxide sensors based on the ZnO nanoflowers

Yang Song, Fang Chen, Yueying Zhang, Sumei Zhang*, Fangmeng Liu, Peng Sun, Xu Yan, Geyu Lu*

State Key Laboratory on Integrated Optoelectronics, Key Laboratory of gas sensors, College of Electronic Science and Engineering, Jilin University, 2699 Qianjin Street, Changchun, Jilin Province 130012, China

ARTICLE INFO

Keywords:
Zinc oxide
Gas sensing
Sensor response
Hydrothermal method
Room temperature
Nitrogen dioxide

ABSTRACT

Herein, ZnO nanoflowers without any doping and modification were synthesized by hydrothermal method. The room temperature nitrogen dioxide sensor with high sensitivity, selectivity and long-term stability was prepared by combining ZnO nanoflowers with interdigital electrodes. The average diameter of the ZnO nanoflowers was about 0.9–1 μm. In addition, the gas sensing properties of the nitrogen dioxide gas sensors at room temperature were investigated. Compared with other ZnO sensors, the sensor based on the ZnO nanoflowers revealed outstanding sensing response to NO_2, giving a response of 0.05–6 ppm. The sensor exhibited a lower detection limit of 0.05 ppm and had an ultra-high response to 1 ppm NO_2 at room temperature. The response was only decreased by 16% of the initial value after 40 days of measurement. The Schottky barrier could be the key factor for the excellent NO_2 sensing properties, which was formed between the Au electrodes and ZnO nanoflowers.

1. Introduction

It is well known that nitrogen dioxide (NO_2) in the air can cause various environmental problems and harm human health [1]. NO_2 can react with gaseous pollutants to form photochemical smog. More seriously, NO_2 can react with water in the air to form acidic solutions, which in turn forms acid rain [2]. These two environmental phenomena seriously affect human life. NO_2 is harmful to human health when the concentration is greater than 3 ppm [3,4]. When NO_2 gas is inhaled by the human, it will produce strong stimulation and corrosion effects on lung tissue, and even cause pulmonary edema. Even 1 ppm of NO_2 can have serious effects on the human organs. Therefore, the lower detection limits are necessary for ideal sensors [5–7]. Nitrogen dioxide is a type of nitrogen oxide that is likely to be primarily produced in human activities and natural behavior [8]. In addition, the detection of NO_2 is essential for air quality control and environmental safety purposes [9]. NO_2 sensors should be developed in the direction of high sensitivity and high selectivity. Therefore, the monitoring of NO_2 has been a long-term important topic.

Usually, the gas sensors need to be heated when they are working. The purpose is to accelerate the process of gas adsorption and extraction to improve the sensitivity and reaction speed of the devices. The ZnO-based sensors typically operate at high working temperatures (typically 200-600℃) [4]. However, high temperature operation has many disadvantages, for example, it tends to increase the energy consumption and reduce the longevity of the devices, which impose great limitations on the large-scale application of the devices. More importantly, when the sensors detect flammable gases, high temperature operation may bring about the risk of gas explosion. Therefore, the society has put forward higher requirements for gas sensors. In addition to higher sensitivity, lower energy consumption, lower cost and other basic requirements, lower operating temperatures are also essential. Consequently, it is important to reduce the operating temperature to room temperature by different methods.

The most common and practical sensors are the metal oxide semiconductor sensors, which have many advantages, such as good working stability, high sensitivity, simple manufacturing process, etc. Common metal oxide semiconductors include ZnO, SnO_2, TiO_2, CuO, Fe_2O_3, WO_3, Ga_2O_3 and V_2O_5 [10–15]. Among all the oxide semiconductors mentioned above, ZnO is known for its wide band gap of 3.37 eV. ZnO has unique properties and broad application prospects, and it has a wide range of applications in sensors, thin film transistors, light-emitting diodes and solar cells [16–18], etc. It is extensively used as a gas sensing material due to its high conductive electron mobility and excellent chemical and thermal stability under sensor operating conditions. Among many gas-sensitive materials, ZnO has attracted the

* Corresponding authors.
E-mail addresses: zsm@jlu.edu.Cn (S. Zhang), lugy@jlu.edu.cn (G. Lu).

https://doi.org/10.1016/j.snb.2019.01.146
Received 8 December 2018; Received in revised form 16 January 2019; Accepted 28 January 2019
Available online 29 January 2019
0925-4005/

attention of many researchers due to its large specific surface area and obvious surface effects. And ZnO sensors have been widely used in the study of a variety of flammable gases and harmful gases. As far as we know, there are few studies on room temperature NO_2 sensors with high response based on pure ZnO materials.

In this paper, the pure ZnO nanoflowers without any doping and modification were prepared by the hydrothermal method. The NO_2 gas sensor was formed by coating ZnO nanoflowers on the interdigital electrodes. The microstructure and morphological properties were analyzed by XRD, XPS, SEM and TEM, respectively. It can be seen from the gas sensing performances that the sensor exhibited good sensing properties to NO_2 at room temperature. Furthermore, a detailed mechanism of the NO_2 reaction was also discussed in the paper. The high response maybe attributed to the Schottky barrier formed by the metal-semiconductor contact.

2. Experimental

2.1. Chemical reagent

All chemicals reagents in the experiment were with analytical reagent grade without further purification and treatment. Zinc nitrate hexahydrate ($Zn(NO_3)_2{\cdot}6H_2O$), glycerol ($C_3H_8O_3$), sodium hydroxide (NaOH) were purchased from Sinopharm Chemical Reagent Co., Ltd. The ethyl alcohol (C_2H_5OH) was purchased from Beijing Chemical Works.

2.2. Synthesis of ZnO nanoflowers

The ZnO nanoflowers were synthesized by hydrothermal method. Glycerol, ethanol and deionized water were blended in a ratio of 7: 7: 10, and the mixture was stirred for 1 h at room temperature to form a transparent solvent. 0.52 *g* of $Zn(NO_3)_2{\cdot}6H_2O$ and 0.8 *g* of NaOH were successively added to the mixed solution under vigorous stirring, and the stirring time was 1 h to ensure uniform mixing. The obtained mixture was transferred into a stainless steel autoclave with a 50 ml Teflon-lined, and then the autoclave was placed in an environment of 120℃ for 12 h. After naturally cooling to room temperature, the obtained precipitates were washed through centrifugation several times with ethanol and distilled water alternately, then the precipitate was dissolved in ethanol and dried at 80℃ for 12 h. And then the white product was collected and annealed at 450℃ for 3 h to obtain ZnO nanoflowers.

2.3. Characterization

The crystal structure of sample was recorded by X-ray diffraction analysis (XRD, scanning speed of 10°/min, scanning range from 20°-80°, using Cu Kα radiation at 0.15418 nm, Rigaku). Field emission scanning electron microscopy (FESEM) on a JSM-7500 F (JEOL) microscope operating at an accelerating voltage of 15 kV was used to observe the size and morphology of the as-prepared products. Transmission electron microscopy (TEM) and high-resolution transmission electron microscopy (HRTEM) observations were carried out on a JEM-2200FS apparatus (JEOL) operating at 200 kV. The surface elemental composition of the as-synthesized samples was studied in detail using X-ray photoelectron spectroscopy (XPS, Thermo ESCALAB 250XI). The absorption spectra was recorded on a SHIMADZU UV-2550 UV-VIS spectrophotometer.

2.4. Fabrication and measurements of gas sensors

The ZnO gas sensor was fabricated by coating the obtained specimens on the interdigital electrodes. The schematic structure of the interdigital electrode is shown in Fig. 1**(a)**. First, the as-synthesized product was ground and mixed with deionized water to form a slurry. Thereafter, the slurry was uniformly coated on the surface of the interdigital electrode with a brush to form a sensing film. The gold interdigital electrodes were prepared on an Al_2O_3 (8×8 mm^2) substrate by the radio frequency magnetron sputtering. The number of the interdigital electrode pairs was 12, the width of the interdigital electrodes was 80 μm, and the distance between the adjacent interdigital electrodes was 70 μm. The gold electrode was composed of Ti/Cu/Ni/Au with a total thickness of 4 μm. The gold electrodes (without the sensor material) on both sides of the interdigital electrode are not in contact, so we believe that the interdigital electrodes are insulated.

After drying in air for 30 min, the well-coated interdigital electrode was calcined at 450℃ for 3 h in the muffle furnace with a heating rate of 3℃/min, in order to improve stability of the sensing film. Except for special notes, the tests were performed at temperature of 25℃ and humidity of 50% RH. The sensing characterization system is as described in Fig. 1**(b)**. A Fluke 8846a (Fluke Co.) was used to record the resistance changes of the sensor in different gases of low concentration, especially in the pristine air and a given amount of the target gases. The maximum recordable measuring resistance of Fluke 8846a is 1000 MΩ. The Hioki SM-8213 resistance meter was used to measure the resistance of 1000–1800 MΩ. When the measured value exceeded 1800 MΩ, the measured value of the instrument was unstable, so only the resistance value below 1800 MΩ was measured. The sensor's response in this paper is defined by parameters R_g/R_a, where R_a and R_g are the resistances of sensor in air and test gas, respectively. In addition, the response time is defined as the time required for the resistance to change to 90% of the total saturation change after the sensor is exposed to the target gas while the recovery time represents the time required for the resistance to return to 10% of the total saturation change after the sensor is released into the air.

3. Results and discussion

3.1. Structure and morphology

The XRD pattern of the obtained ZnO sample is shown in Fig. 2. It can be seen from the figure that all diffraction peaks of the obtained material could be matched with the PDF standard card of hexagonal wurtzite ZnO (JCPDS Card No. 5-664). The diffraction peaks at 31.78, 34.46, 36.28, 47.58, 56.58, 62.90, 66.42, 67.94, 69.08, 72.62 and 76.96° could be assigned to (100), (002), (101), (102), (110), (103), (200), (112), (201), (004), and (202) planes of hexagonal wurtzite ZnO, respectively. The lattice parameters of the above-mentioned wurtzite ZnO were a = 3.249 Å, b = 3.249 Å, c = 5.205 Å. No other peaks were found in the XRD pattern, which indicated that the as-prepared ZnO had high purity and good crystallinity.

The UV–vis absorption spectrum of the prepared ZnO sample is shown in Fig. 3. The UV–vis absorption spectra of the pure ZnO nanoflowers (shown in Fig. 3**(a)**) showed a clear absorption shoulder in the UV region (300–400 nm), which was the band edge absorption of the pure ZnO materials. It can be seen that the ZnO sample had less absorption in the visible region. From the absorption spectrum, the optical band gap (E_g) of the obtained ZnO could be estimated from the Tauc's formula by [19] :

$$\alpha h\nu = B(h\nu\text{-}E_g)^n \quad (1)$$

Where α is the optical absorption coefficient, h is Planck constant, ν is the frequency of incident photons and B is a constant. By consulting the literature, it is known that the value of n depends on the type of the transition in the semiconductor. When the measured material belongs to an indirect transition, n = 2, while when it belongs to a direct transition, n = 1/2 [20]. According to the above instructions, the n value of ZnO is determined to be 1/2. As shown in the Fig. 3**(b)**, the band gap of ZnO nanoflowers is about 3.19 eV. This value is lower than the value (3.37 eV) for most reported ZnO, which may be due to the structural defects in the preparation of materials.

XPS was used to examine the chemical state of elements and

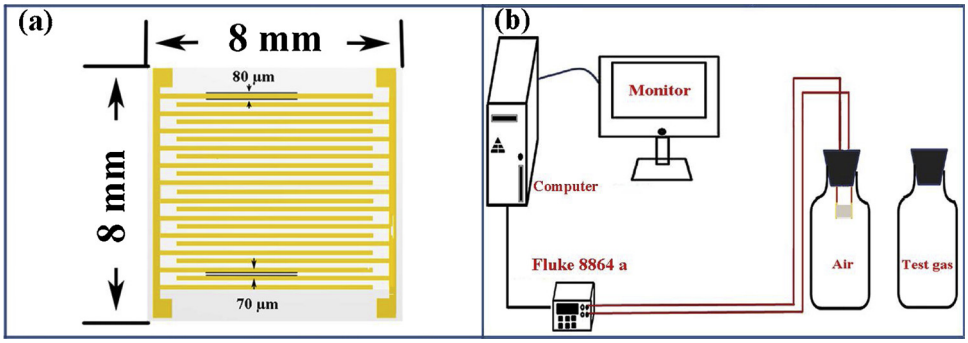

Fig. 1. (a) Schematic diagram of the interdigital electrode; (b) Schematic diagram of the sensing characterization system.

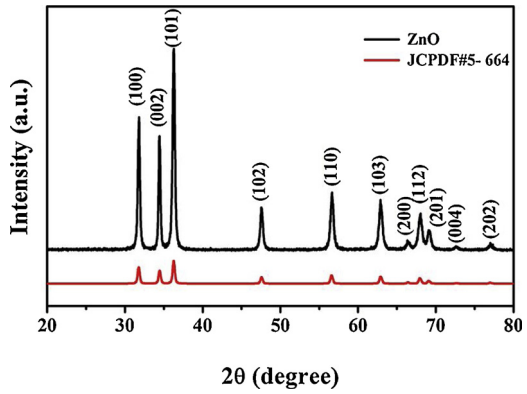

Fig. 2. XRD patterns of the PDF 5–664 data and ZnO.

chemical composition of the ZnO samples. As shown in Fig. 4**(a)**, full range XPS peaks corresponding to C, O and Zn was clearly observed in the survey spectrum. Furthermore, we can see that there are no other peaks except the target peak, which indicated that no impurity elements were introduced into the samples. All binding energies in the XPS analysis required charge correction, with a standard peak of C (284.5 eV) as the calibration peak [21]. The XPS spectrum of Zn 2p (shown in Fig. 4**(b)**) was divided into two peaks, corresponding to the Zn $2p_{1/2}$ and Zn $2p_{3/2}$ states of Zn 2p orbits, respectively. The two fitted peaks were respectively located at 1021.86 and 1044.87 eV, which were ascribed to Zn^{2+} in wurtzite ZnO. As for O 1 s spectrum in Fig. 4**(c)**, it was corresponded to three type oxygen species (the lattice oxygen O_L, defective oxygen (oxygen vacancies) O_V and the chemisorbed oxygen species O_C). The central positions and the relative percentages of the three type oxygen species were shown in Table 1. The relatively high percentage of defective oxygen species component means that the oxygen vacancies are abundant in the sample. This is consistent with previous reports that the metal oxides prepared hydrothermally under alkaline conditions are prone to produce oxygen vacancies [22,23]. The chemisorbed oxygen species leaded to a great improvement of the oxygen absorption capacity, which enhances the response with the target gas and leads to good gas sensing performance as a sensing material [24].

The morphological structures of the ZnO samples obtained after calcination are shown in Fig. 5. The pure ZnO product displayed a flower-like structure gathered with tens of nanorods. The length of these nanorods varied from 250 to 400 nm, and the nanorods were substantially tapered. As shown in Fig. 5**(a)**, the size of the ZnO nanoflowers was uniform. The SEM image in Fig. 5**(b)** indicated that the average diameter of the flower-like architecture was 0.9–1 μm.

The TEM images of the ZnO nanoflowers are showed in Fig. 6, which revealed the refined structures of products. Fig. 6**(a)** is the TEM image of two ZnO nanoflowers, and the illustration is the partial enlarged view of the nanoflowers. It could be clearly seen that the wrinkles on the surface of the samples. Fig. 6**(b)** shows the high resolution TEM (HRTEM) image of the prepared ZnO samples. The ordered lattice fringes of wurtzite hexagonal phase ZnO were observed. Ordered lattice fringes of wurtzite hexagonal phase ZnO were observed with a lattice spacing of 0.28 nm, corresponding to the (100) lattice plane of ZnO (JCPDS No. 5-664).

3.2. Gas sensing properties

In this research, all gas sensing property tests were carried out at room temperature, except for working temperature measurement. Fig. 7**(a)** showed the dependence of resistance of the sensor on the temperature in the dry air (humidity of 21% RH). As with surface controlled sensors, the resistance of the sensors decreased with increasing temperature [25]. The response to 1 ppm NO_2 at 25℃-107℃ is shown in Fig. 7**(b)**. The sensor exhibited the maximum response at 25℃. With the increase of operating temperature, NO_2 molecules began to desorb, resulting in a decrease in gas response. The effect of humidity on the gas-sensing performance of the ZnO nanoflowers sensor was investigated. As shown in Fig. 7**(c)**, we measured the response to 1 ppm

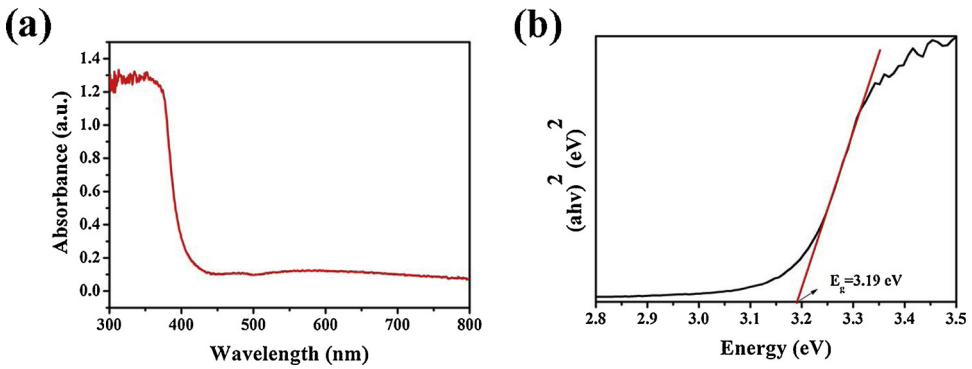

Fig. 3. (a) The UV–vis absorption spectrum of the ZnO; (b) The estimated band gap energy of ZnO.

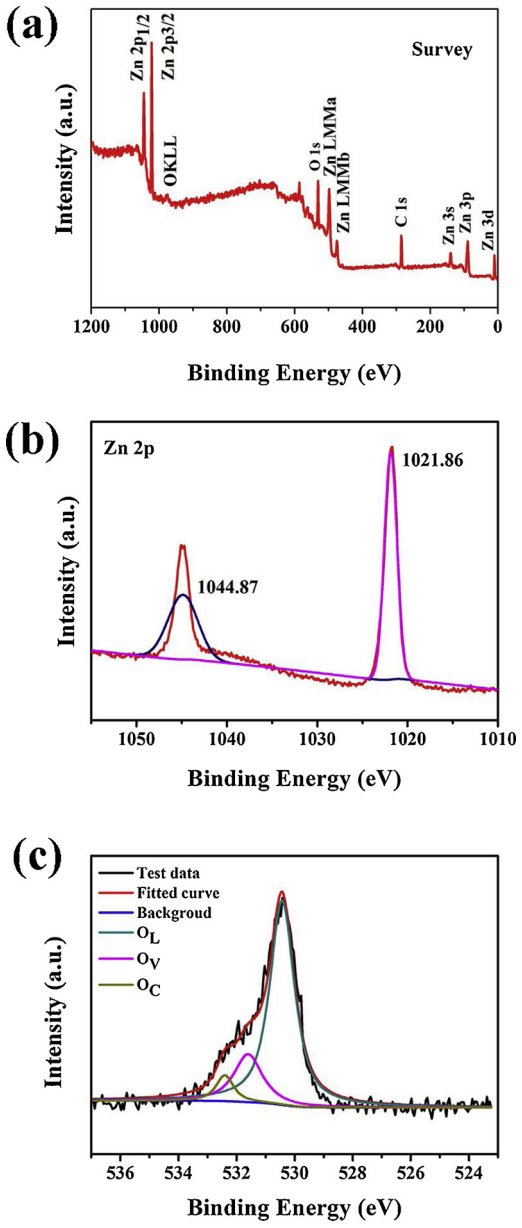

Fig. 4. XPS patterns of ZnO nanoflowers; (a) XPS survey of scan spectrum; (b) Zn 2p of ZnO nanoflowers; (c) O 1 s of ZnO nanoflowers.

NO_2 in the humidity range of 25%–70%. The results showed that with the increase of humidity, the reaction gradually increased. Fig. 7**(d)** exhibits the response of the sensor to NO_2, giving the response of 0.05–6 ppm. When the concentration of NO_2 is more than 6 ppm, the resistance of the sensor exceeded the measurable range of the instrument. The response gradually increased with the increase of NO_2 concentration. What's more, the ZnO-based gas sensor exhibited a very good linear relationship between the response and concentration within the measurable range. The response curve of the sensor at low concentration is shown as the inset of Fig. 7**(d)**.

The dynamic gas sensing transients of the ZnO nanoflowers-based sensor to different concentrations of NO_2 are exhibited in Fig. 8**(a)**. When the concentration of NO_2 is 50 ppb, the response of the sensor could reach 3.44, which indicated a low detection limit. Fig. 8**(b)** shows the three reversible cycles of the sensor to 1 ppm NO_2, which revealed that the satisfying stability and repeatable of the sensor based on the ZnO nanoflowers. The response time and recovery time of the ZnO nanoflowers sensor (shown in Fig. 8**(c)**) were approximately 6 and 4 min, respectively. The response time and recovery time at different NO_2 concentrations could be seen in the Table. 2. It can be found that the recovery time is longer at low concentrations, which may be related to the difficulty in desorption of NO_2 at low concentrations. The long-term stability of the gas sensor is also a very important parameter of the gas sensors. In order to test the stability, we collected the response data of ZnO-based gas sensors to 1 ppm NO_2 for 40 days. As shown in Fig. 8**(d)**, the response was only decreased by 16% of the initial value after 40 days of measurement. The reduction of gas response with the number of days may be due to the influence of humidity on the sensor [26]. This illustrated that the ZnO-based sensor is a promising candidate for the detection of NO_2 gas in the field of gas sensors.

Table. 3 displayed a comparison between the present sensor and the other ZnO room temperature sensors which were reported in the previous literature. It is obvious that the sensor possessed high response, which was superior to most of the reported ZnO room temperature sensors. In addition, the detection limit (50 ppb) is also much lower than other reported sensors. The comparison indicated the sensor had a broad application prospect in NO_2 detection at room temperature.

Selectivity of the sensor is a key factor to evaluate the gas-sensing properties of semiconductor materials for practical applications. Fig. 9 shows the selectivity measurements of the ZnO-based sensor to 1 ppm different gases, such as nitrogen dioxide (NO_2), carbon monoxide (CO), methane (CH_4), ammonia (NH_3) and acetone (CH_3COCH_3). Selective study of different tested gases showed that the response of the ZnO nanoflowers sensor to NO_2 was obviously better than that of other gases. It can be seen that the response to NO_2 was much higher than other gases, which was almost 15 times larger than NH_3 and 20 times larger than CO. It demonstrated that the selectivity of the sensor to NO_2 was much superior.

3.3. Discussion of NO_2 sensing mechanism

The gas sensing mechanism of the ZnO sensors can be well illustrated from two aspects, one is the gas sensing property of ZnO nanoflowers, the other is the depletion layer variation caused by the Schottky barrier, which is formed by the metal-semiconductor contact [19]. When ZnO nanoflowers contact with air, the surface of each tapered ZnO column will form an electron depletion layer, forming a narrow conduction channel. When the sensor is in contact with NO_2 gas, the sensitive layer loses more electrons, which leads to a wider depletion layer and a thinner conduction channel, resulting in the measurable changes in resistance. It can be seen from the Fig. 5**(a)**, the ZnO nanoflowers cross each other, allowing the electrons to move freely throughout the whole sensitive layer. This flower-like structure allows the sensitive layer to have more voids, so that the NO_2 gas molecules have more adsorption sites in the entire sensitive layer. According to the theoretical framework of the oxide semiconductor gas sensor established by N. Yamazoe [33], the porosity of the sensitive

Table 1
Fitting Results of O 1 s XPS Spectra of the pure ZnO nanoflowers.

Sample	Oxygen Species	Binding Energy (eV)	Relative percentage (%)
Pure ZnO nanoflowers	O_L (Zn-O)	530.431	73.7
	O_V (Vacancy)	531.600	19.7
	O_C (Chemisorbed)	532.402	6.6

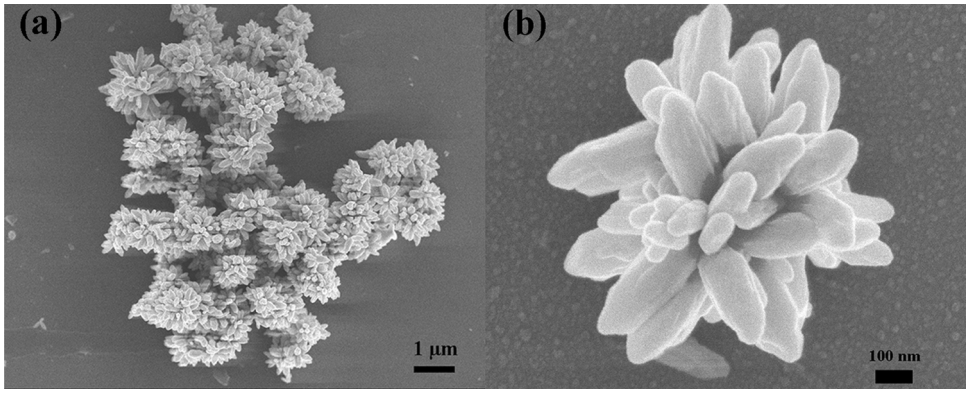

Fig. 5. SEM images of ZnO nanoflowers.

layer can make the utilization efficiency of the sensitive body higher, resulting in an improvement in sensor performance. Therefore, the flower structure is part of the reason for the high response of the sensor.

When the ZnO was uniformly coated on the surface of the interdigital electrodes, the Schottky barrier is formed between the ZnO and Au electrodes, resulting in an increase in the thickness of the electron depletion layer at the Au electrodes/ZnO interface. And the superior response to NO_2 at room temperature may be due to the decrease in the activation energy of chemical adsorption on the gas surface [34]. Similarly, the reason for the longer recovery time of ZnO sensors at room temperature is that the activation energy of gas desorption is much higher than that of thermal energy [35].

Oxygen molecules in the air will be physically-adsorbed on the surface of the ZnO nanoflowers, and electrons will be captured from the adsorption sites on the surface of ZnO to produce different chemisorbed oxygen species at different temperatures [36]. The oxygen ions are mainly existed in the form of O_2^- at room temperature. The reactions of eqn.(2) ~ (3) occur on the surface of ZnO as follows:

$$O_{2(gas)} \rightarrow O_{2(ads)} \quad (2)$$

$$O_{2(ads)} + e^- \rightarrow O_{2(ads)}^- \quad (3)$$

where O_2^- is the oxygen adsorption, e^- are electrons [37,38]. It can be seen that the above reactions capture free electrons from ZnO to produce chemical adsorption oxygen species. The absorbed oxygen molecules on the surface of ZnO act as an acceptor, resulting in a decrease in the amount of electrons in the conduction band, thereby changing the resistivity of the sample. When the sensor is exposed to other tested gases, its resistance will also change. And the change in resistance increases with the increase of gas concentration [37,38].

The adsorption of oxygen leads to the formation of the built-in potential barrier and the electron depletion layer on the surface of ZnO material, as shown in Fig. 10 [39,40]. The dark gray area in the figure is the depletion layer of ZnO in the air. The light gray area is the increased width of the depletion layer when the sensor is transferred to NO_2. There is a certain relationship between the depletion width (L) and the built-in potential barrier (V), which can be expressed by formula (4) [41]:

$$L = \left(\frac{2\varepsilon V}{qN_d}\right)^{\frac{1}{2}} \quad (4)$$

where ε is the dielectric constant of ZnO, q is the electron charge, and N_d is the donor density.

Because the work functions of Au and ZnO are not equal, the work functions of Au and ZnO are 5.1 eV and 4.45 eV respectively [44–46]. Electrons in ZnO occupy higher energy levels than those in Au. The electrons in ZnO will cross to Au to equal the two Fermi levels. Because of the transfer of electrons, an electron depletion layer is formed at the interface between ZnO and Au. The energy band of ZnO bents upward to form a barrier to prevent electrons from crossing to Au, i.e. Schottky barrier. When ZnO contacts with the gold electrodes, more electrons are transferred to the gold electrode, thus forming a wider electron depletion layer and a higher built-in potential barrier, as shown in Fig. 10 [47–49]. In addition, the oxygen species are more easily adsorbed on the surface of Au electrode [50], capturing free electrons in ZnO and producing more chemisorbed oxygen, so the contact of Au electrode with ZnO will accelerate the reaction and improve the performance of sensor.

NO_2 is higher than O_2 in terms of electron affinity, which makes NO_2 possess higher electrophilicity [42,43]. The property can make more electrons in the conduction band of ZnO transfer to NO_2. In addition, O_2^- has high activity and is easy to react with other types of gases, which is conducive to gas interaction. When the sensor is exposed to NO_2, the NO_2 molecules will occupy on the sensor to form physisorbed NO_2:

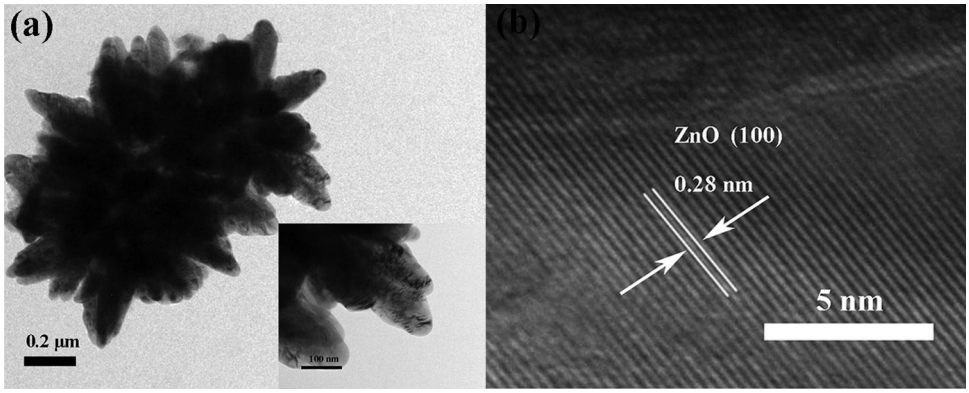

Fig. 6. (a) TEM images of ZnO sample; (b) HRTEM images of ZnO sample.

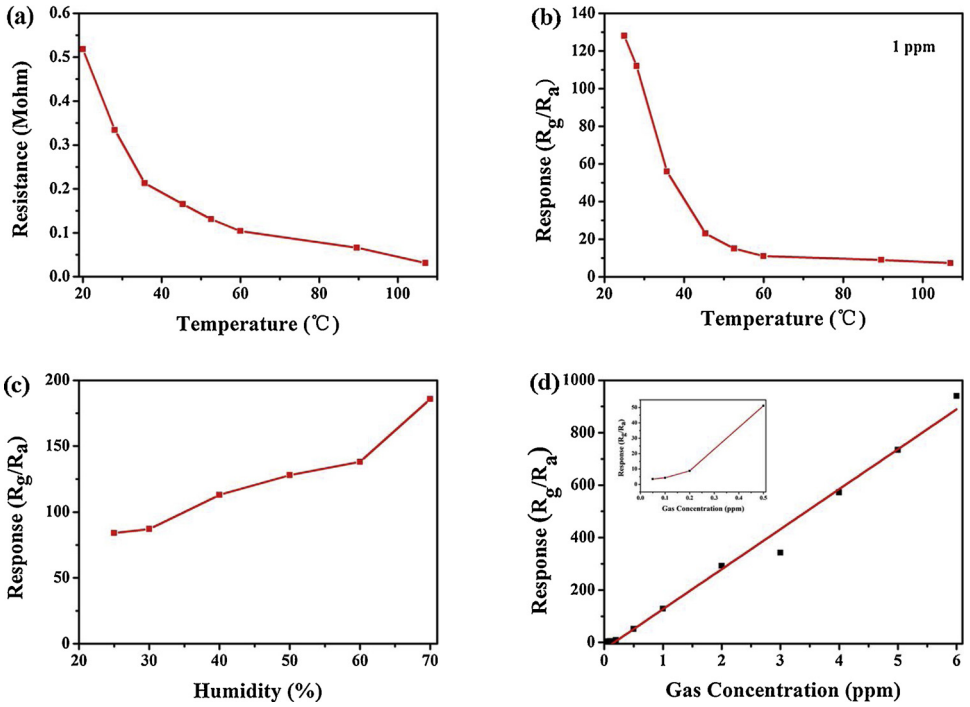

Fig. 7. (a) The dependence of resistance of the sensor on the temperature in the dry air (humidity of 21% RH); (b) The response to 1 ppm NO_2 at different operation temperatures; (c) The effect of humidity on the response of the ZnO nanoflowers sensor to 1 ppm NO_2 at room temperature; (d) Response to different concentrations of NO_2 at room temperature (The inset is the response curve at low concentration).

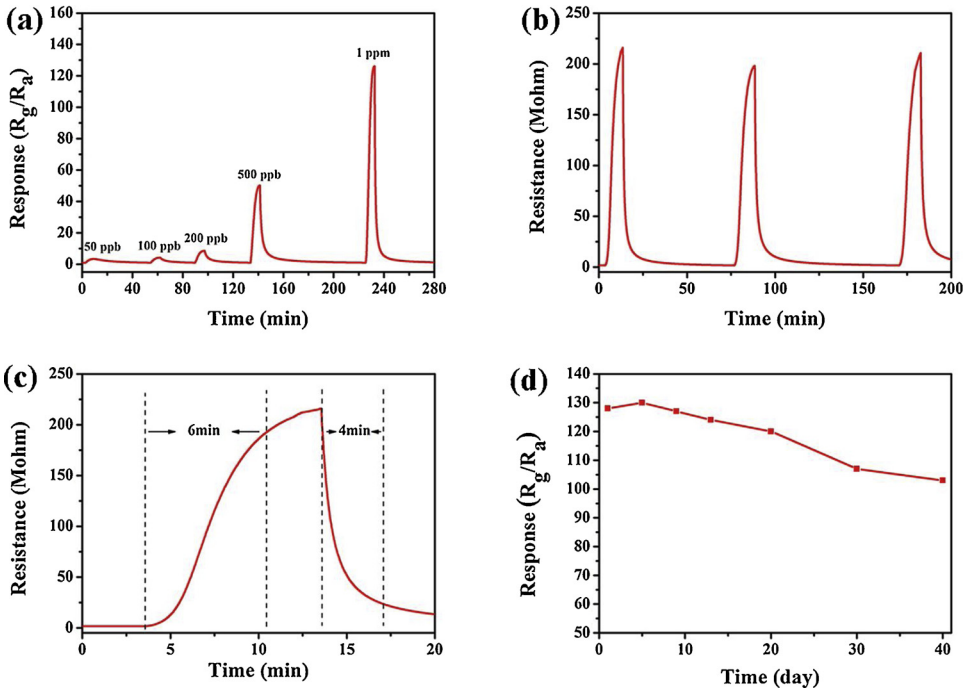

Fig. 8. (a) Dynamic response of ZnO under increasing NO_2 exposure at room temperature; (b) The three reversible cycles of response and recovery curves of the sensor to 1 ppm NO_2 at room temperature; (c) Dynamic response of ZnO to 1 ppm of NO_2 at room temperature; (d) Stability measurements of ZnO sensor to 1 ppm NO_2 at room temperature within 40 days.

Table 2
Response time and recovery time at different NO_2 concentrations.

NO_2 concentration (ppm)	Response	Response time (min)	Recovery time (min)
0.05	3.44	3	44
0.1	4.265	5	16
0.2	8.75	5	4
0.5	51.14	5	6
1	128.55	6	4

$$NO_{2(gas)} \rightarrow NO_{2(ads)}$$

Moreover, NO_2 will capture electrons and react with adsorbed oxygen species to produce adsorbed $NO_{2(ads)}^-$, which can be commentated as follows:

$$NO_{2(ads)} + e^- \rightarrow NO_{2(ads)}^- \quad (5)$$

$$NO_{2(ads)} + O_{2(ads)}^- + 2e^- \rightarrow NO_{2(ads)}^- + 2O_{(ads)}^- \quad (6)$$

In addition, XPS spectra showed that there are abundant double donor defects (Zn interstitial and O vacancy) in the samples. The donor defects can effectively reduce the surface adsorption energy, improve the surface activity and greatly increase the density of surface

Table 3
Comparison of the sensing performance of the present sensor and that of devices reported in the previously literature (RT denotes room temperature).

Sensing material	Method	NO_2 concentration (ppm)	Working temperature (°C)	Response	detection limit(ppm)	Reference
Mesoporous ZnO sheets	Precipitation-calcination method	1	RT	2.3	1	[4]
Ultrathin ZnO nanorods	Hydrothermal method	1	RT	2	1	[27]
ZnO nanowires	Chemical vapor deposition	20	RT	32	5	[28]
Polycrystalline ZnO	Sol–gel method	20	RT	2.2	20	[29]
ZnO nanoparticles/ rGO	Wet chemical method	5	RT	1.256	5	[30]
Hierarchical ZnO nanorods/PbS quantum dots	Wet chemical method	1	RT (under NIR illumination)	2.22	1	[31]
ZnO nanosheets/ porous silicon	Electrochemical deposition	1	RT	< 6	0.1	[32]
ZnO nanoflowers	Hydrothermal method	1	RT	128	0.05	This work

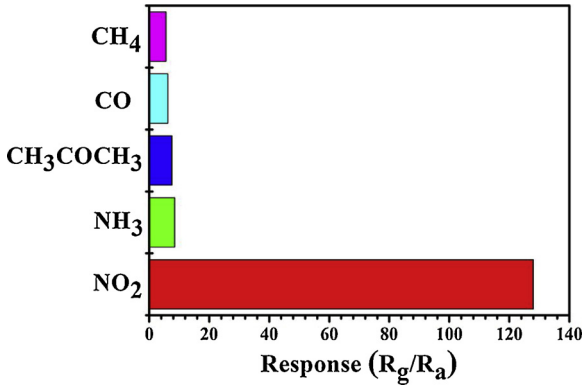

Fig. 9. Selectivity measurements of the ZnO sensor to 1 ppm of NO_2 and other typical gases at room temperature.

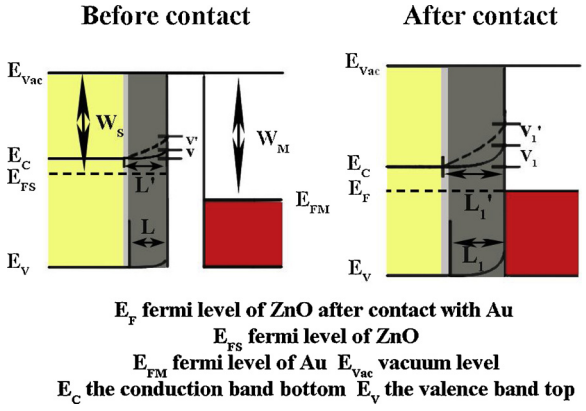

Fig. 10. Schematic of the mechanism and the energy band structure at the interface of ZnO and Au.

adsorption sites. It would result in the increasing of the built-in potential barrier and the depletion layer, which make the resistance of the sensor reaches a maximum value, and finally the sensor produces an ultrahigh response to NO_2.

Furthermore, the application of the interdigital electrodes can reduce the initial resistance of the gas sensor. The operating principle of sensor is that the change of resistance value of sensor corresponds to the change of gas concentration. Therefore, the selection of initial resistance value of sensor is critical. If the initial resistance value of sensor is too large in the working environment, it is likely to be affected by environmental factors. Especially when the equivalent resistance value of surrounding air is equal to the resistance value of sensor, the measurement of components will be inaccurate. The application of interdigital electrodes can effectively reduce the initial resistance value of sensor under working conditions, and it can also effectively increase the rate of chemical reaction and accelerate the process of establishing reaction, thus improving the performance of sensors and shortening the reaction time. It turns out that the application of the interdigital electrode does reduce the resistance of the sensor. Different from the sensor in this paper, the resistance of the sensor fabricated on ceramic tubes with the same material is beyond our measurement range. Therefore, this paper can bring a new idea for sensor resistance reduction and realization of room temperature sensor.

4. Conclusions

The ZnO nanoflowers without any doping and modification were synthesized by hydrothermal method. When the ZnO samples were uniformly coated on the surface of the interdigital electrode, the Schottky barrier was formed between ZnO and Au electrodes, which may be the reason why the sensor exhibited excellent NO_2-sensing properties. The response of the sensor to 1 ppm NO_2 could achieve 128 at room temperature. And the detection limit of the NO_2 sensor was merely 50 ppb. More importantly, when the concentration of NO_2 is 50 ppb, the response of the sensor can still reach 3.44. The NO_2 gas sensor had a quite high response and good selectivity. The application and development of sensors composed of interdigital electrodes and semiconductors will attract widespread attention in the field of gas sensors.

Acknowledgments

This work is supported by the National Key Research and Development Program (No. 2016YFC0207300). National Nature Science Foundation of China (No. 61831011, No. 61722305, No. 61503148, No. 61520106003 and No. 61327804). Science and Technology Development Program of Jilin Province (No. 20170520162JH). China Postdoctoral Science Foundation funded project (No. 2017T100208 and No. 2015M580247).

References

[1] S.T. Navale, A.T. Mane, M.A. Chougule, R.D. Sakhare, S.R. Nalage, V.B. Patil, Highly selective and sensitive room temperature NO_2 gas sensor based on polypyrrole thin films, Synth. Met. 189 (2014) 94–99.
[2] S. Bai, J. Guo, J. Sun, P. Tang, A. Chen, R. Luo, D. Li, Enhancement of NO_2-sensing performance at room temperature by graphene-modified polythiophene, Ind. Eng. Chem. Res. 55 (2016) 5788–5794.
[3] J.A. Bernstein, N. Alexis, C. Barnes, I.L. Bernstein, A. Nel, D. Peden, D. Diaz-Sanchez, S.M. Tarlo, P.B. Williams, Health effects of air pollution, J. Allergy Clin. Immunol. 114 (2004) 1116–1123.
[4] R. Chen, J. Wang, L. Xiang, Facile synthesis of mesoporous ZnO sheets assembled by small nanoparticles for enhanced NO_2 sensing performance at room temperature, Sens. Actuators B Chem. 270 (2018) 207–215.
[5] A.M. Andringa, C. Piliego, I. Katsouras, P. Blom, D. Leeuw, NO_2 detection and real-time sensing with field-effect transistors, Chem. Mater. 26 (2014) 773–785.
[6] L. Huang, Z. Wang, J. Zhang, J. Pu, Y. Lin, S. Xu, L. Shen, Q. Chen, W. Shi, Fully

printed, rapid-response sensors based on chemically modified graphene for detecting NO_2 at room temperature, ACS Appl. Mat. Interfaces 6 (2014) 7426–7433.
[7] Z. Dai, H. Dai, Y. Zhou, D. Liu, G. Duan, W. Cai, Y. Li, Monodispersed $Nb2O_5$ microspheres: facile synthesis, air/water interfacial self-assembly, $Nb2O_5$-based composite films, and their selective NO2 sensing, Adv. Mater. Interfaces 2 (2015) 1–7.
[8] M. Breedon, M.J.S. Spencer, I. Yarovsky, Adsorption of NO and NO_2 on the ZnO (2 1 1 0) surface: a DFT study, Surf. Sci. 603 (2009) 3389–3399.
[9] S. Zampolli, I. Elmi, J. Stürmann, S. Nicoletti, L. Dori, G. Cardinali, Selectivity enhancement of metal oxide gas sensors using a micromachined gas chromatographic column, Sens. Actuators B Chem. 105 (2005) 400–402.
[10] J. Zeng, M. Hu, W. Wang, H. Chen, Y. Qin, NO_2-sensing properties of porous WO_3 gas sensor based on anodized sputtered tungsten thin film, Sens. Actuators B Chem. 161 (2012) 447–452.
[11] S. Maeng, S.W. Kim, D.H. Lee, S.E. Moon, K.C. Kim, A. Maiti, SnO_2 nanoslab as NO_2 sensor: identification of the NO_2 sensing mechanism on a SnO_2 surface. ACS Appl, Mater. Interfaces 6 (2013) 357–363.
[12] S.A. Vanalakar, V.L. Patil, N.S. Harale, S.A. Vhanalaker, M.G. Gang, J.Y. Kim, P.S. Patil, J.H. Kim, Controlled growth of ZnO nanorod arrays via wet chemical route for NO_2 gas sensor applications, Sens. Actuators B Chem. 221 (2015) 1195–1201.
[13] M. Epifani, R. Díaz, J. Arbiol, E. Comini, N. Sergent, T. Pagnier, P. Siciliano, G. Faglia, J.R. Morante, Nanocrystalline metal oxides from the injection of metal oxide sols in coordinating solutions: synthesis, characterization, thermal stabilization, device processing, and gas-sensing properties, Adv. Funct. Mater. 16 (2006) 1488–1498.
[14] Y.H. Navale, S.T. Navale, N.S. Ramgir, F.J. Stadler, S.K. Gupta, D.K. Aswal, V.B. Patil, Zinc oxide hierarchical nanostructures as potential NO_2 sensors. Sens, Sens. Actuators B Chem. 251 (2017) 551–563.
[15] E. Şennik, S. Kerli, Ü Alver, Z.Z. Ozturk, Effect of fluorine doping on the NO_2-sensing properties of ZnO thin films, Sens. Actuators B Chem. 216 (2015) 49–56.
[16] Y. Shi, M. Wang, C. Hong, Z. Yang, J. Deng, X. Song, L. Wang, J. Shao, H. Liu, Y. Ding, Multi-junction joints network self-assembled with converging ZnO nanowires as multi-barrier gas sensor, Sens. Actuators B Chem. 177 (2013) 1027–1034.
[17] X. Zhang, M. Lu, Y. Zhang, L. Chen, Z. Wang, Fabrication of a high-brightness blue-light-Emitting diode using a ZnO-Nanowire array grown on p-GaN thin film, Adv Mater 21 (2009) 2767–2770.
[18] B. Xiang, P. Wang, X. Zhang, S.A. Dayeh, D.P. Aplin, C. Soci, D. Yu, D. Wang, Rational synthesis of p-type zinc oxide nanowire arrays using simple chemical vapor deposition, Nano Lett. 7 (2007) 323–328.
[19] N. Srinatha, Y.S. No, V.B. Kamble, S. Chakravarty, N. Suriyamurthy, B. Angadi, A.M. Umarji, W.K. Choi, Effect of RF power on the structural, optical and gas sensing properties of RF-sputtered Al doped ZnO thin films, RSC Adv. 6 (2016) 9779–9788.
[20] G.K. Pradhan, D.K. Padhi, K.M. Parida, Fabrication of α-Fe_2O_3 nanorod/RGO composite: a novel hybrid photocatalyst for phenol degradation, ACS Appl. Mater. Inter. 5 (2013) 9101–9110.
[21] C. Wang, T.S. Wang, B.Q. Wang, X. Zhou, X.Y. Cheng, P. Sun, J. Zheng, G.Y. Lu, Design of alpha-Fe_2O_3nanorods functionalized tubular NiO nanostructure for discriminating toluene molecules, Sci. Rep. 6 (2016) 26432.
[22] B. Xu, Q. Zhang, S. Yuan, M. Zhang, T. Ohno, Synthesis and photocatalytic performance of yttrium-doped CeO_2 with a porous broom-like hierarchical structure, Appl. Catal. B: Environ. 183 (2016) 361–370.
[23] B. Xu, Q. Zhang, S. Yuan, S. Liu, M. Zhang, T. Ohno, Synthesis and photocatalytic performance of yttrium-doped CeO_2 with a hollow sphere structure, Catal. Today 281 (2017) 135–143.
[24] X. Cheng, Z. Rong, X. Zhang, Y. Xu, S. Gao, H. Zhao, L. Huo, In situ assembled ZnO flower sensors based on porous nanofibers for rapid ethanol sensing, Sens. Actuators B Chem. 188 (2013) 425–432.
[25] S. Wei, S. Wang, Y. Zhang, M. Zhou, Different morphologies of ZnO and their ethanol sensing property, Sens. Actuators B Chem. 192 (2014) 480–487.
[26] P.S. Shewale, G.L. Agawane, S.W. Shin, A.V. Moholkar, J.Y. Lee, J.H. Kim, M.D. Uplane, Thickness dependent H_2S sensing properties of nanocrystalline ZnO thin films derived by advanced spray pyrolysis, Sens. Actuators B Chem. 177 (2013) 695–702.
[27] Y. Xia, J. Wang, X. Li, D. Xie, D. Zhou, L. Xiang, S. Komarneni, Nanoseed-assisted rapid formation of ultrathin ZnO nanorods for efficient room temperature NO_2 detection, Ceram. Int. 42 (2016) 15876–15880.
[28] X. Pan, X. Zhao, J. Chen, A. Bermaka, Z. Fan, A fast-response/recovery ZnO hierarchical nanostructure based gas sensor with ultra-high room-temperature output response, Sens. Actuators B Chem. 206 (2015) 764–771.
[29] S.W. Fan, A.K. Srivastava, V.P. Dravid, Nanopatterned polycrystalline ZnO for room temperature gas sensing, Sens. Actuators B Chem. 144 (2010) 159–163.
[30] S. Liu, B. Yu, H. Zhang, T. Fei, T. Zhang, Enhancing NO_2 gas sensing performances at room temperature based on reduced graphene oxide-ZnO nanoparticles hybrids, Sens. Actuators B Chem. 202 (2014) 272–278.
[31] R. Chen, J. Wang, Y. Xia, L. Xiang, Near infrared light enhanced room-temperature NO_2 gas sensing by hierarchical ZnO nanorods functionalized with PbS quantum dots, Sens. Actuators B Chem. 255 (2018) 2538–2545.
[32] D. Yan, M. Hu, S. Li, J. Liang, Y. Wu, S. Ma, Electrochemical deposition of ZnO nanostructures onto porous silicon and their enhanced gas sensing to NO_2 at room temperature, Electrochim. Acta 115 (2014) 297–305.
[33] N. Yamazoe, G. Sakai, K. Shimanoe, Oxide semiconductor gas sensors, Catal. Surv. Asia 7 (2003) 63–75.
[34] D.E. Motaung, I. Kortidis, G.H. Mhlongo, M.M. Duvenhage, H.C. Swart, G. Kiriakidisc, S.S. Ray, Correlating the magnetism and gas sensing properties of Mn-doped ZnO films enhanced by UV irradiation, RSC Adv. 6 (2016) 26227–26238.
[35] Z. Wang, G. Men, R. Zhang, F. Gu, D. Han, Pd loading induced excellent NO_2 gas sensing of 3DOM In_2O_3 at room temperature, Sens. Actuators B Chem. 263 (2018) 218–228.
[36] S. Bai, K. Zhang, R. Luo, D. Li, A. Chen, C.C. Liu, Low-temperature hydrothermal synthesis of WO_3 nanorods and their sensing properties for NO_2, J. Mater. Chem. 22 (2012) 12643–12650.
[37] Nilam B. Patil, Amol R. Nimbalkar, Maruti G. Patil, ZnO thin film prepared by a sol-gel spin coating technique for NO_2 detection, Mater. Sci. Eng. B 227 (2018) 53–60.
[38] K. Arshak, I. Gaidan, Development of a novel gas sensor based on oxide thick films, Mater. Sci. Eng., B 118 (2005) 44–49.
[39] Q. Yang, X. Cui, J. Liu, J. Zhao, Y. Wang, Y. Gao, P. Sun, J. Ma, G. Lu, A low temperature operating gas sensor with high response to NO_2 based on ordered mesoporous Ni-doped In_2O_3, New J. Chem. 40 (2016) 2376–2382.
[40] J. Zhang, Z. Qin, D. Zeng, C. Xie, Metal-oxide-semiconductor based gas sensors: screening, preparation, and integration, Phys. Chem. Chem. Phys. 19 (2017) 6313–6329.
[41] M.-W. Ahn, K.-S. Park, J.-H. Heo, D.-W. Kim, K.J. Choi, J.-G. Park, On-chip fabrication of ZnO-nanowire gas sensor with high gas sensitivity, Sens. Actuators B Chem. 138 (2009) 168–173.
[42] P. Li, H. Fan, Y. Cai, M. Xu, C. Long, M. Li, S. Lei, X. Zou, Phase transformation (cubic to rhombohedral): the effect on the NO_2 sensing performance of Zn-doped flower-like In_2O_3 structures, RSC Adv. 4 (2014) 15161–15170.
[43] Y. Itagaki, M. Mori, Y. Hosoya, H. Aono, Y. Sadaoka, O_3 and NO_2 sensing properties of $SmFe_{1-x}Co_xO_3$ perovskite oxides, Sens. Actuators B Chem. 122 (2007) 315–320.
[44] U.T. Nakate, R.N. Bulakhe, C.D. Lokhande, S.N. Kale, Au sensitized ZnO nanorods for enhanced liquefied petroleum gas sensing properties, Appl. Surf. Sci. 371 (2016) 224–230.
[45] Y.J. Fang, J. Sha, Z.L. Wang, Y.T. Wan, W.W. Xia, Y.W. Wang, Behind the change of the photoluminescence property of metal-coated ZnO nanowire arrays, Appl. Phys. Lett. 98 (2011) 033103.
[46] Z. Shen, X. Zhang, X. Ma, R. Mi, Y. Chen, S. Ruan, The significant improvement for BTX (benzene, toluene and xylene) sensing performance based on Au-decorated hierarchical ZnO porous rose-like architectures, Sens. Actuators B Chem. 262 (2018) 86–94.
[47] B. Liu, D. Cai, Y. Liu, D. Wang, L. Wang, Strongly coupled hybrid nanostructures for selective hydrogen detection–understanding the role of noble metals in reducing cross-sensitivity, Nanoscale 6 (2014) 4758–4764.
[48] D.X. Ju, H.Y. Xu, Z.W. Qiu, Z.C. Zhang, Q. Xu, J. Zhang, J.Q. Wang, B.Q. Cao, Near room temperature, fast-response, and highly sensitive triethylamine sensor assembled with Au-Loaded ZnO/SnO_2 core–shell nanorods on flat alumina substrates, ACS Appl. Mater. Interfaces 7 (2015) 19163–19171.
[49] Y. Yang, C. Tian, L. Sun, R. Lu, W. Zhou, K. Shi, K. Kan, J. Wang, H. Fu, Growth of small sized CeO_2 particles in the interlayers of expanded graphite for high-performance room temperature NO_x gas sensors, J. Mater. Chem. A Mater. Energy Sustain. 1 (2013) 12742–12749.
[50] H.-J. Kim, J.-H. Lee, Highly sensitive and selective gas sensors using p-type oxide semiconductors: overview, Sens. Actuators B Chem. 192 (2014) 607–627.

Yang Song received the B.Eng. degree in department of electronic science and technology in 2017. He is currently studying for his M.E. Sci. degree in College of Electronic Science and Engineering, Jilin University, China.

Fang Chen received the B.Eng. degree from the Electronics Science and Engineering department in 2017. She is currently studying for her M.E. Sci. degree in College of Electronic Science and Engineering, Jilin University, China.

Yueying Zhang received the B.Eng. degree in department of electronic science and technology in 2017. She is currently studying for her M.E. Sci. degree in College of Electronic Science and Engineering, Jilin University, China.

Sumei Zhang received her PhD from Jilin University of China in 2005. Presently, she is working as associate professor in Electronics Science and Engineering department of Jilin University. Her current research interests are nanoscience and gas sensors.

Fangmeng Liu received his PhD degree in 2017 from College of Electronic Science and Engineering, Jilin University, China. Now he is a lecturer of Jilin University, China. His current research interests include the application of functional materials and development of solid state electrolyte gas sensor and flexible device.

Peng Sun received his PhD degree from College of Electronic Science and Engineering, Jilin University, China in 2014. He was appointed the lecturer in Jilin University in the same year. Now, he is engaged in the synthesis and characterization of the semiconducting functional materials and gas sensors.

Xu Yan received his M.S degree in 2013 from Nanjing Agricultural University. He joined the group of Prof. Xingguang Su at Jilin University and received his pH.D. degree in June 2017. Since then, he did postdoctoral work with Prof. Geyu Lu and Prof. Junqiu Liu. Currently, his research interests mainly focus on the development of the functional nanomaterials for chem/bio sensors.

Geyu Lu received the B. Sci. degree in electronic sciences in 1985 and the M.S. degree in 1988 from Jilin University in China and the Dr. Eng. degree in 1998 from Kyushu University in Japan. Now he is a professor of Jilin University, China. His current research interests include the development of chemical sensors and the application of the function materials.